Electronic Research Archive

http://www.aimspress.com/journal/era

ERA, 34(3): 1653–1670.
DOI: 10.3934/era.2026075
Received: 15 December 2025
Revised: 09 February 2026
Accepted: 11 February 2026
Published: 27 February 2026

Research article

A deep learning-based model for the propagation mechanism of southern corn rust

Keqin Su[1], Alain Miranville[2,3], Jie Cao[1] and Xinguang Yang[2,*]

[1] College of Information and Management Science, Henan Agricultural University, China
[2] Department of Mathematics and Statistics, Henan Normal University, Xinxiang 453007, China
[3] Laboratoire de Mathématiques Appliqués du Havre, Université Le Havre Normandie, Le Havre 76600, France

* **Correspondence:** Email: yangxinguangyxg@163.com.

Abstract: A new mathematical model based on differential equations and deep learning is proposed to study the propagation mechanism of southern corn rust (SCR). Equilibrium and stability analyses of system are conducted in detail. Compared with the quantitative assessment of SCR, numerical parameter estimation and the corresponding interpretation are given.

Keywords: southern corn rust; mathematical modeling; deep learning

1. Introduction

Southern corn rust (SCR), caused by *puccinia polysora*, is one of the most devastating corn diseases, in which the pathogen is an obligate biotrophic parasite. In recent years, the disease has become prevalent globally, and it is very difficult to control because of its wide distribution, long-distance migration, and fast evolution, all of which significantly increase the risk of an epidemic. *Puccinia polysora* was first described and named by Underwood in 1897 [1]. In China, SCR was first identified in Hainan Province in 1972 [2]. According to statistical data from the Center for Agriculture and Bioscience International, the disease has spread to over 110 countries.

The large-scale outbreak of SCR in the core US corn belt resulted in 30–50% yield losses during 1972–1974. In the 1900s, disease surveys confirmed that SCR had become one of the major diseases of corn, causing yield losses of up to 40% in susceptible corn varieties [3]. Due to the large-scale cultivation of susceptible varieties and favorable climatic conditions for disease development, the impact of SCR in China has shown a persistent worsening trend [4]. The outbreak of SCR in 2015 was particularly severe: the affected area reached 5.289 million hectares, with yield losses as high as 756 million kilograms [5]. Corn is one of the most important food and feed crops globally, SCR often

reduces corn yield and quality, and the annual yield loss of corn due to SCR has increased significantly.

Puccinia polysora infects, grows, and reproduces only on living corn plant tissues, primarily targeting above-ground parts such as leaves, leaf sheaths, and stems [6]. Temperature and humidity are the most critical factors influencing spore germination, infection, and disease spread. The temperature range for the occurrence and progression of SCR is 15–31°C, with the most favorable temperatures for spore germination and disease development being 26–28 °C and 24–27 °C, respectively [7], and the uredinia of *puccinia polysora* primarily develop on the upper leaf surface. Urediniospores are the primary infection source causing SCR. The formation of urediniospores from a single uredinium can persist for 18–20 days, releasing approximately 2000 and 1150 spores daily from susceptible and resistant plants, respectively [8]. Typhoons act as key drivers of the spores' spread over long distances, and the landing pathway and duration of their stay directly determine the epidemic range and severity of SCR [9].

Compared with human and animal infections, the application of mathematical models to plants is less frequent, and the relating interesting results can be referred to [10–13]. Moreover, the mathematical methods used for plant infections include the disease progress curve, disease cycle models, and differential equations, which describe the infection process and measure the severity of plant disease. For specific conclusions, see [14–16].

Differential equations constitute a highly applied branch of mathematics, which has attracted sustained attention from many researchers and established a comprehensive theoretical framework. They are useful tools to study the epidemic patterns, pathogenesis, and predictions of plant diseases. Differential equations not only characterize information transfer between compartments but also describe the rate of change for each variable, which are very useful in understanding the occurrence and transmission mechanisms of diseases among humans and animals [17–19]. For example, the susceptible-infected-recovered (SIR) and susceptible-exposed-infected-recovered (SEIR) models, stability theory, and numerical simulation are used to study the dynamic behavior of systems [20, 21], and we can refer to [22–24] for the latest research findings. However, differential equations have yielded limited results in plant disease research, particularly regarding SCR infection and the disease's spread.

In light of the summary of analytical methods for plant epidemics, we comprehensively consider the actual infection and reproduction of corn rust fungus, and the background of corn plants' growth. We use differential equations to model the spread of SCR and achieve a deep understanding of its kinetic mechanisms. Using the susceptible-exposed-infected (SEI) model, we modify it, integrate the transmission factors of SCR, and form a new system. A study of the stability, parameter estimation, and fitting are also made correspondingly.

In summary, the specific objectives of this study are to: (i) construct a biologically plausible ordinary differential equation (ODE) model (SEI) that captures the latent and infectious periods of SCR; (ii) utilize a deep-learning-based segmentation method (YOLOv11) to extract the precise time-series data of infected leaf areas from experimental images; and (iii) bridge the gap between theoretical modeling and experimental data by estimating the key parameters, specifically introducing a time-varying transition rate to reflect the pathogen's incubation process.

This article is arranged as follows. The modified SEI model involving SCR's spread is given in Section 2, and equilibrium and stability analyses are given. A quantitative assessment of SCR using

YOLOv11 semantic segmentation is presented in Section 3. Numerical parameter estimation, an interpretation, and a discussion are provided finally.

2. Mathematical model and qualitative analysis: the SCR-based SEI model

This section will construct the mathematical model and present a theoretical analysis for our problem.

2.1. Mathematical modeling

The propagation of SCR involves distinct biological stages: healthy tissue, latent infection (incubation), and sporulation. To translate this biological process into a mathematical framework, we adopt a compartmental modeling approach. We partition the total corn leaf area into three compartments as follows:

(1) **Susceptible ($S(t)$):** the proportion of healthy corn leaf area that can be infected by spores.
(2) **Exposed/Latent ($E(t)$):** the proportion of leaf area the *puccinia polysora* has invaded and hyphae are growing internally, but no external symptoms (uredinia) are visible. This corresponds to the early stage of infection characterized by increased biomass.
(3) **Infected ($I(t)$):** the proportion of leaf area showing visible symptoms (erupted uredinia) and that is capable of releasing spores to infect susceptible tissue.

Based on the transmission mechanism of SCR, healthy tissue S transitions to the exposed state E upon contact with spores from infected tissue I (or partially from latent tissue due to internal hyphal spread). Subsequently, after an incubation period, the latent tissue E becomes infectious I. The following differential equations are proposed to describe this dynamics:

$$\begin{cases} \dfrac{dS(t)}{dt} = \Lambda - \beta S(t)(I(t) + \theta E(t)) - \mu S(t), \\ \dfrac{dE(t)}{dt} = \beta S(t)(I(t) + \theta E(t)) - (\sigma + \mu)E(t), \\ \dfrac{dI(t)}{dt} = \sigma E(t) - (\delta + \mu)I(t), \end{cases} \tag{2.1}$$

where Λ is the recruitment rate of susceptible tissue, μ is the natural loss rate of system, β is the transmission rate (day^{-1}), θ represents the relative infectivity of latent individuals compared with infectious ones (dimensionless), σ is the rate at which latent individual become infected, and δ is the removal rate of infected individuals (day^{-1}).

2.2. Equilibrium points

In this part, we consider the equilibrium points (the disease-free equilibrium point and the endemic equilibrium point). Since the solution of the system must be biologically meaningful, we choose the following positively invariant set:

$$D = \{(S, E, I) | S, E, I \in [0, 1]\}$$

as the domain of the system, and the disease-free equilibrium point is

$$\left(S_*,\ E_*,\ I_*\right) = \left(\frac{\Lambda}{\mu},\ 0,\ 0\right).$$

To derive the endemic equilibrium point (S^*, E^*, I^*), we consider the following system

$$\begin{cases} 0 = \Lambda - \beta S^*(I^* + \theta E^*) - \mu S^*, \\ 0 = \beta S^*(I^* + \theta E^*) - (\sigma + \mu)E^*, \\ 0 = \sigma E^* - (\delta + \mu)I^*. \end{cases} \tag{2.2}$$

After calculation, we obtain

$$S^* = \frac{(\delta + \mu)(\mu + \sigma)}{\beta(\theta(\delta + \mu) + \sigma)}, \tag{2.3}$$

$$E^* = \frac{\Lambda\beta(\theta(\delta + \mu) + \sigma) - \mu(\delta + \mu)(\mu + \sigma)}{\beta(\mu + \sigma)(\theta(\delta + \mu) + \sigma)}, \tag{2.4}$$

$$I^* = \frac{\sigma}{\delta + \mu}E^*. \tag{2.5}$$

From the expressions above, we know the endemic equilibrium point exists uniquely.

2.3. Basic reproduction number

The basic reproduction number (R_0) is a core epidemiological index that represents the average number of healthy cells an infected cell can infect during its entire infectious period. In the following, we use the next-generation matirx method to derive the basic reproduction number of the system.

Let $(E, I)^T$ represent the vector of infectious compartments. We decompose the system as $F - V$, where F represents the new infection term and V represents the transition and removal. At (S_*, E_*, I_*), we obtain

$$F = \begin{pmatrix} \beta S_*\theta & \beta S_* \\ 0 & 0 \end{pmatrix}, \quad V = \begin{pmatrix} \sigma + \mu & 0 \\ -\sigma & \delta + \mu \end{pmatrix}.$$

Then the next-generation matrix is $K = FV^{-1}$, and its spectral radius $\rho(K)$ gives the basic reproduction number

$$R_0 = \rho(K) = \beta S_*\left(\frac{\theta}{\sigma + \mu} + \frac{1}{\delta + \mu}\right) = \beta\frac{\Lambda}{\mu}\left(\frac{\theta}{\sigma + \mu} + \frac{1}{\delta + \mu}\right). \tag{2.6}$$

Remark 2.1. Given the endemic equilibrium point and basic reproduction number, we find that

$$S^* > 0, E^* > 0, I^* > 0 \iff \Lambda\beta(\theta(\delta + \mu) + \sigma) - \mu(\delta + \mu)(\mu + \sigma) > 0 \iff R_0 > 1.$$

which is the relation between the existence of a positive endemic equilibrium point and the basic reproduction number, and has biological significance.

In the context of SCR, R_0 represents the average area of healthy leaf tissue that a unit area of infected tissue can successfully infect during its entire infectious period in a completely susceptible corn field. From Eq (2.6), we observe that R_0 is proportional to the transmission rate β and the duration of the infectious period $1/(\delta + \mu)$. This provides a theoretical basis for disease control: reducing β (e.g., via fungicides or controlling humidity) or shortening the infectious period is critical to driving $R_0 < 1$ and suppressing the epidemic.

2.4. Stability property

Theorem 2.2. *If $R_0 \leq 1$, the system is locally asymptotically stable at (S_*, E_*, I_*), and this is not the case when $R_0 > 1$.*

Proof. At $(S_*, E_*, I_*) = (\Lambda/\mu, 0, 0))$, we calculate the Jacobian matrix as follows:

$$J_* = \begin{pmatrix} -\mu & -\beta S_*\theta & -\beta S_* \\ 0 & \beta S_*\theta - (\sigma+\mu) & \beta S_* \\ 0 & \sigma & -(\delta+\mu) \end{pmatrix},$$

where

$$\begin{vmatrix} \beta S_*\theta - (\sigma+\mu) & \beta S_* \\ \sigma & -(\delta+\mu) \end{vmatrix} > 0 \iff R_0 < 1.$$

This means that $R_0 < 1$ is the sufficient and necessary condition on the locally asymptotical stability of the system, since three eigenvalues are negative. This is not the case when $R_0 > 1$. □

Theorem 2.3. *If $R_0 > 1$, the system is locally asymptotically stable at (S^*, E^*, I^*).*

Proof. At (S^*, E^*, I^*), we calculate the Jacobian matrix as follows:

$$J^* = \begin{pmatrix} -\beta(I^* + \theta E^*) - \mu & -\beta S^*\theta & -\beta S^* \\ \beta(I^* + \theta E^*) & \beta S^*\theta - (\sigma+\mu) & \beta S^* \\ 0 & \sigma & -(\delta+\mu) \end{pmatrix}.$$

We use the Routh-Hurwitz method to show the locally asymptotical stability. We denote the characteristic polynomial as

$$f(\lambda) = \lambda^3 + \xi_1\lambda^2 + \xi_2\lambda + \xi_3,$$

where

$$\begin{aligned} \xi_1 &= -tr(J^*) \\ &= -(-\beta(I^* + \theta E^*) - \mu + \beta S^*\theta - (\sigma+\mu) - (\delta+\mu)) \\ &= \beta((I^* + \theta E^*) - S^*\theta) + (\sigma + \delta + 3\mu). \end{aligned}$$

By imposing a restriction on the term $\beta((I^* + \theta E^*) - S^*\theta)$, ξ_1 can be made positive. Given that ξ_2 is the sum of all principal minors of order two, we can show that $\xi_2 > 0$ when $R_0 > 1$. We also have

$$\xi_3 = -|J^*| = \begin{vmatrix} -\beta(I^* + \theta E^*) - \mu & -\beta S^*\theta & -\beta S^* \\ \beta(I^* + \theta E^*) & \beta S^*\theta - (\sigma+\mu) & \beta S^* \\ 0 & \sigma & -(\delta+\mu) \end{vmatrix}.$$

Expanding the determinant along the first row, we can show that $\xi_3 > 0$ and $\xi_1\xi_2 > \xi_3$ when $R_0 > 1$. According to the Routh-Hurwitz criterion, we can derive the locally asymptotical stability of the system at the (S^*, E^*, I^*). □

Theorem 2.4. *If $R_0 \leq 1$, the system is globally asymptotically stable at (S_*, E_*, I_*), and it is unstable if $R_0 > 1$.*

Proof. If we take $Z = (E, I)^T$ for the infected compartments, we construct the Lyapunov function as follows

$$L(E, I) = aE + bI,$$

where the parameters a, b are to be determined, and we derive

$$\begin{aligned}\frac{dL}{dt} &= a\frac{dE}{dt} + b\frac{dI}{dt}\\ &= a\left(\beta S\left(I + \theta E\right) - (\sigma + \mu)E\right) + b\left(\sigma E - (\delta + \mu)I\right)\\ &= \left(a\beta S\,\theta - a(\sigma + \mu) + b\sigma\right)E - \left(a\beta S\, - b(\delta + \mu)\right)I.\end{aligned}$$

It follows that the sufficient and necessary condition on the globally asymptotical stability at (S_*, E_*, I_*) is

$$\begin{aligned}\frac{dL}{dt} \le 0 \Leftrightarrow &\begin{cases} a\beta S_*\theta - a(\sigma + \mu) + b\sigma \le 0\\ a\beta S_* - b(\delta + \mu) \le 0\end{cases}\\ &\Leftrightarrow (\delta + \mu)(\sigma + \mu) \ge \beta S_*(\theta(\delta + \mu) + \sigma)\\ &\Leftrightarrow R_0 \le 1.\end{aligned}$$

Thus, we finish the proof. □

Remark 2.5. If $R_0 \le 1$, the Lyapunov function is decreasing, which means that the infection variable does not grow indefinitely and eventually declines to zero. It is worth noting that the global asymptotic stability established here naturally implies the local asymptotic stability presented in Theorem 2.2. However, the linearization analysis in Theorem 2.2 is retained, as it explicitly provides the spectral properties of the Jacobian matrix, which is standard for analyzing the threshold dynamics. If $R_0 > 1$, $\frac{dL}{dt} > 0$ holds in some domain, and the infection variable will increase and converge to an endogenous steady state.

2.5. Numerical illustration

To provide a comprehensive understanding of the long-term dynamics of SCR and address the stability of the equilibrium points, we perform numerical simulations for four distinct scenarios: $R_0 = 0.8, 1.0, 2.0$, and 4.0. For each scenario, three different initial conditions are considered: $P_1(0.9, 0.1, 0.0)$, $P_2(0.8, 0.2, 0.0)$, and $P_3(0.7, 0.3, 0.0)$. These points represent varying degrees of latent infection in a newly exposed corn field where visible symptoms (I) have not yet appeared. The phase portraits in the (S, I) plane are illustrated in Figure 1.

The following are illustrated in Figure 1:

(1) **Disease-free scenarios ($R_0 \le 1$):** in the cases of $R_0 = 0.8$ and $R_0 = 1.0$, regardless of the initial proportions of susceptible and latent tissues, all trajectories converge to the disease-free equilibrium (DFE) $E_0 = (1, 0, 0)$. This numerical evidence complements Theorem 2.2, confirming the global attractivity of E_0. Biologically, this suggests that if control measures effectively limit R_0 below unity, the SCR epidemic will eventually be eradicated from the field.

(2) **Endemic scenarios ($R_0 > 1$):** for $R_0 = 2.0$ and $R_0 = 4.0$, the DFE becomes unstable, and all trajectories starting from the three different initial states are attracted to a unique strictly positive endemic equilibrium (S^*, E^*, I^*). As R_0 increases, the equilibrium value of I^* shifts upward, indicating a higher steady-state disease severity.

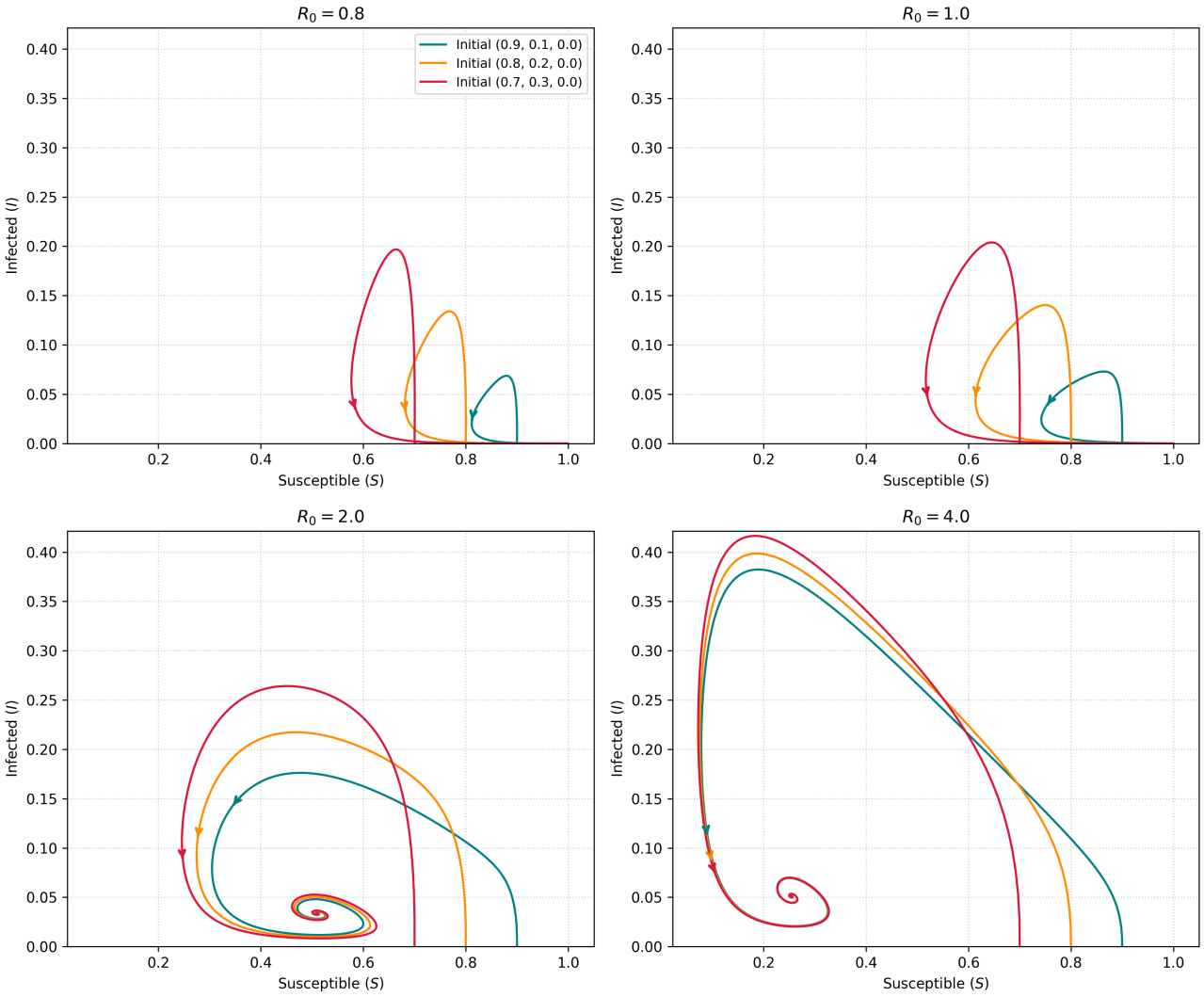

Figure 1. Phase portraits of $I(t)$ vs. $S(t)$.

Importantly, the fact that all trajectories from distinct regions of the phase space converge to the same (S^*, E^*, I^*) provides strong numerical evidence for the global asymptotic stability of the endemic equilibrium when $R_0 > 1$. This extends our analytical results in Theorem 2.3, which establishes local stability. Mathematically, this global attraction suggests the absence of periodic orbits or limit cycles in the system. Practically, it implies that the SCR infection will persist at a predictable, constant level determined by the system's parameters, reinforcing the reliability of our model for long-term disease forecasting.

3. Quantitative assessment of SCR

To fit the model, in what follows, we collect experimental data in two phases, namely the the early stage and the middle to late stage of infection, and then perform unified processing. To ensure

the reliability of the model, we utilize actual experimental data derived from artificial inoculation of *puccinia polysora* on corn leaves.

3.1. Quantitative assessment during the early stage of infection

As an obligate, biotrophic and parasitic filamentous fungus, *puccinia polysora* invades the tissue through stomata of corn leaves and continuously grows and reproduces. During the early stage of infection, the phenotypic changes in corn leaves are subtle, and the reproductive propagation of SCR cannot be effectively characterized through phenotypic analysis. Nevertheless, the intercellular hyphae of the pathogen elongate extensively and produce branches; secrete a large quantity of effector proteins to suppress immunity of the host simultaneously, thereby establishing a parasitic relationship, and the biomass of pathogens within the leaf also increases significantly. In a statistical sense, we can characterize the reproductive trends of SCR infection during the early stage by experimentally measuring the biomass ratio in the leaves (Table 1).

Table 1. Biomass ratio over days.

Day	Biomass ratio
1	0.244541671
2	0.303654098
3	0.404220168
4	0.611024305
5	0.737043899
6	0.960282220
7	0.966386529
8	0.940761718
9	0.956353148
10	0.963203114

3.2. Quantitative assessment during the middle to late stage of infection

In the middle infection stage, the expansion of the pathogen slows down, which primarily utilizes its specialized hyphal structures (called haustoria) to continuously absorb nutrients from the corn cells, preparing for subsequent reproductive growth. In the middle to late stage of infection, the intercellular hyphae accumulate in a cushion-like manner beneath the epidermis of the host, where the hyphal cells participate in forming urediniospores. These urediniospores serve as a secondary inoculum to infect adjacent healthy corn plants, and the cycle repeats continuously, which leads to large-scale epidemics of SCR. During the middle to late stage of fungal development, the growth of biomass slows as resources are allocated to reproductive growth and spore formation. At this time, we need to conduct precise detection of diseased corn leaves to investigate the progression of SCR in its middle to late stages. The traditional phenotypic analysis methods have drawbacks, such as being time-consuming and subjective, which can be effectively addressed by deep learning technology; in particular, instance segmentation offers efficient solutions for automated disease analysis, and the YOLOv11 model is exactly what we need.

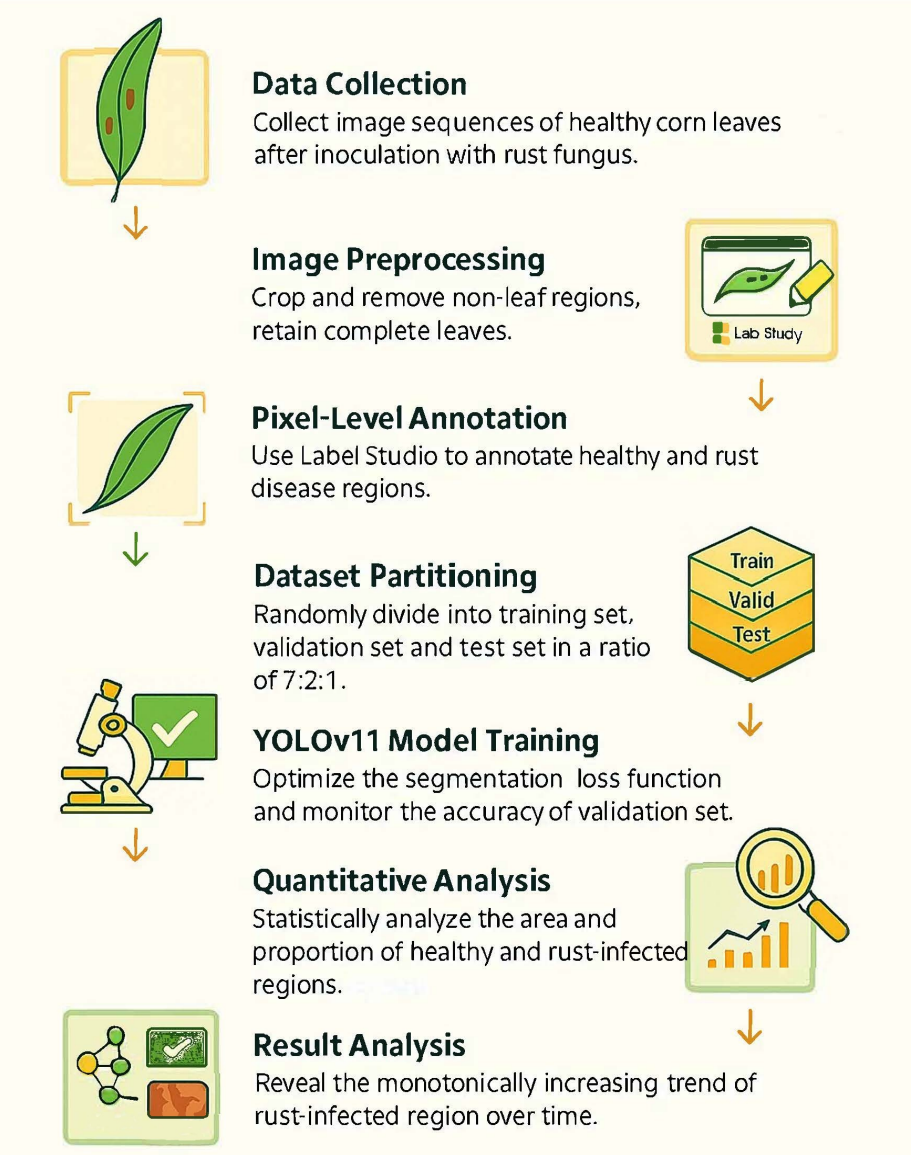

Figure 2. Technical roadmap for temporal analysis of corn leaf rust infection.

3.2.1. Data collection and preprocessing

Following artificial inoculation with *puccinia polysora*, we collected phenotypic images of corn leaves for 11 consecutive days, starting from the fifth day after inoculation. To eliminate background interference and accentuate the pathological features, a rigorous preprocessing pipeline was implemented. Non-leaf regions were precisely excised through image cropping techniques, and only the intact leaves were retained. Subsequently, pixel-level semantic segmentation annotations were performed using Label Studio, which allowed the healthy and rust-infected regions on each leaf to be carefully distinguished and annotated. This process provided critical ground truth labels for model training in boundary-precise feature learning.

(a) Day 6 **(b)** Day 10 **(c)** Day 14

Figure 3. Phenotypic images of corn leaves after preprocessing.

3.2.2. Dataset partitioning and model training

The annotated image dataset was randomly partitioned into three parts, namely the training set, validation set, and test set in a ratio of 7 : 2 : 1. This allocation ensured sufficient training data volume while reserving independent subsets for hyperparameter tuning and performance evaluation.

The YOLOv11 instance segmentation model was selected as the core algorithmic framework due to its efficiency in object detection and pixel-level segmentation, which make it particularly suitable for segmenting irregular rust areas against complex backgrounds. The model iteratively learns by optimizing the segmentation loss function on the training set, and simultaneously monitors the segmentation accuracy metrics (e.g., mean intersection over union) of the validation set to select the optimal model weights and ensure robust generalizability.

3.2.3. Time series analysis

The trained YOLOv11 model is used to perform automatic inference on image sequence of the same leaf from the test set, and generate segmentation masks that distinguish healthy versus rust-infected regions. Through pixel counting on these masks, we can compute the absolute areas of healthy and rust-affected regions at each timepoint and the proportion of rust-affected area to total leaf area. Since no directly observable infected areas were detected during the first five days, the proportions of rust-infected area from Day 6 to Day 15 obtained by this method are presented in the I_{obs} column of Table 3.

The automated segmentation results revealed the clear temporal pattern of rust disease's progression. After inoculation, both the absolute area and the relative proportion of rust-infected regions exhibited a significant and monotonically increasing trend, and quantitative results are consistent with the hypothesis of rust disease's spread over time, which provides reliable data for disease dynamics research.

4. Numerical parameter estimation

According to the conventional practices in mathematical epidemiology [25], we treat σ as a constant, study the corresponding autonomous system to establish the dynamical behavior of SCR, and derive the equilibrium points, the basic reproduction number, and the relating conditions on stability. Under these circumstances, some particular techniques such as the next-generation method and the Lyapunov functional method are used, which are usually more complex or not directly applicable for non-autonomous systems [26]. In addition, environmental fluctuation and experimental

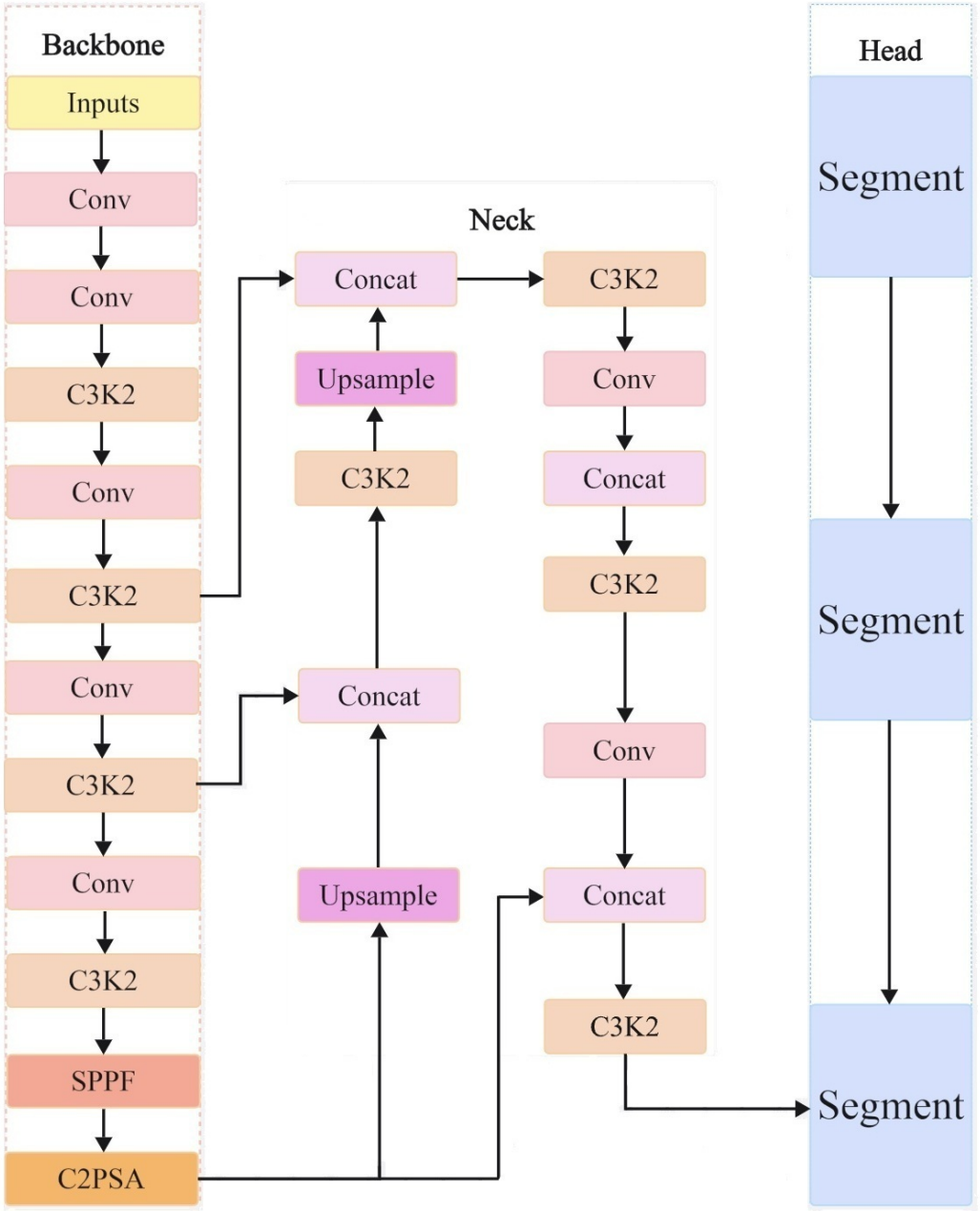

Figure 4. The YOLOv11 instance segmentation model.

errors can lead to instability in the experimental data, which poses significant challenges for subsequent data fitting.

In the following, we replace σ by a time-varying term $\sigma(t)$ in logistic form to capture the dynamic mode, which can reflect the delay in biological maturation of the pathogen within the host tissue. Biologically, *puccinia polysora* requires a specific incubation period to develop from the initial hyphal invasion to sporulation. Consequently, the transition rate from the latent stage E to the infectious stage I is not constant; it remains low during the incubation phase and rises sharply when the fungal pustules mature and erupt synchronously.

(a) Day 6 **(b)** Day 10 **(c)** Day 14

Figure 5. The automated segmentation results of the trained YOLOv11 model.

This modeling strategy allows us to capture the dynamic mode of a sharp increase in infected tissue after a slow latent buildup. This modeling strategy aligns with practices in both human and plant epidemiology. That is, we examine an autonomous system with a constant rate σ first and then extend to the non-autonomous case with a time-dependent rate $\sigma(t)$ to adapt to the environmental forcing and stage-dependent changes of the pathogens [27, 28].

In this situation, the theoretical threshold in the autonomous case is typically considered as the structural descriptor of the infection process, whereas the time-varying property in the non-autonomous case reflects the non-equilibrium experimental dynamics. Therefore, we consider the following modified SEI system:

$$\begin{aligned} \frac{dS(t)}{dt} &= \Lambda - \beta S(t)(I(t) + \theta E(t)) - \mu S(t), \\ \frac{dE(t)}{dt} &= \beta S(t)(I(t) + \theta E(t)) - \sigma(t)\, E(t) - \mu E(t), \\ \frac{dI(t)}{dt} &= \sigma(t)\, E(t) - (\delta + \mu) I(t), \end{aligned} \tag{4.1}$$

where

$$\sigma(t) = \frac{\sigma_{\max}}{1 + \exp(-\eta(t - \tau))}$$

is a logistic-type function representing a smooth increase from the latent to the infected category over time. Here, $\sigma_{\max}$ is the maximum asymptotic value of the rate at which latent individuals become infectious (day^{-1}), τ is the midpoint time of the logistic transition curve for the rate at which latent individuals become infectious, and η is the steepness parameter controlling the abruptness of the transition in the conversion rate from the latent to the infectious state.

4.1. Fitted parameters

In this part, we will fit the parameters $(\beta, \theta, \sigma_{\max}, \tau)$ of $\sigma(t)$ to the experimental data collected from Day 1 to Day 15. The fixed parameters are set to $\mu = 1/100$, $\Lambda = \mu$, and $\delta = 1/7$, based on the biological conditions of leaf senescence and the infected period. The steepness parameter of the logistic-type transition rate is fixed at $\eta = 1.0$ to avoid overparameterization.

Table 2 summarizes the parameter estimates, the approximate standard errors derived from the local Jacobian of the least-squares problem, and the confidence intervals.

Table 2. Estimated parameters of SEI model with $\sigma(t)$.

Parameter	Estimate	Std. Error	95% CI (lower)	95% CI (upper)
β	2.9832	0.3682	2.2397	3.7267
θ	0.1993	0.0161	0.1667	0.2319
$\sigma_{\max}$	0.6000	0.1781	0.2404	0.9596
τ	8.9393	0.6029	7.7218	10.1568

The overall root-mean-square error (RMSE) of the fit across the three compartments is

$$\mathrm{RMSE}_{\mathrm{overall}} = 0.1028,$$

which indicates a good global match between the model and the experimental time-series data.

4.2. Comparison between observation and model prediction

Table 3 lists the observed values and the corresponding model predictions for $S(t)$, $E(t)$, and $I(t)$ for each day. The fitted curves show two key qualitative features of experimental data. The first is the slow growth of $I(t)$ during the first 5–6 days, and the second is the rapid rise from Day 7 onward.

Table 3. Observed data and fitted model predictions.

Day	S_{obs}	S_{pred}	E_{obs}	E_{pred}	I_{obs}	I_{pred}
1	0.755458	0.755458	0.244542	0.244542	0	10^{-9}
2	0.696346	0.633548	0.303654	0.366337	0	0.0001085
3	0.595780	0.492339	0.404220	0.507103	0	0.0005137
4	0.388976	0.353078	0.611024	0.644786	0	0.0019382
5	0.262956	0.235465	0.737044	0.757248	0	0.0065483
6	0.039718	0.147667	0.959960	0.829632	0.000323	0.020231
7	0.033613	0.086929	0.963830	0.848751	0.002557	0.056791
8	0.059238	0.046645	0.887339	0.793329	0.053422	0.139308
9	0.043647	0.022265	0.536631	0.649636	0.419722	0.278436
10	0.036797	0.010686	0.400727	0.456912	0.562476	0.432441
11	0.033334	0.006708	0.302779	0.286834	0.663887	0.537720
12	0.033334	0.005676	0.239475	0.171234	0.727191	0.576143
13	0.033334	0.005597	0.193687	0.102188	0.772979	0.566114
14	0.033334	0.005889	0.154131	0.063116	0.812535	0.530036
15	0.033334	0.006385	0.121425	0.041445	0.845241	0.483131

4.3. Interpretation of estimated parameters

Here, $\tau \approx 8.94$ indicates that the latent-to-infectious conversion rate $\sigma(t)$ begins its sharp logistic increase near Day 9, which aligns with the observed onset of a rapid increase in infected tissue around Day 7–8.

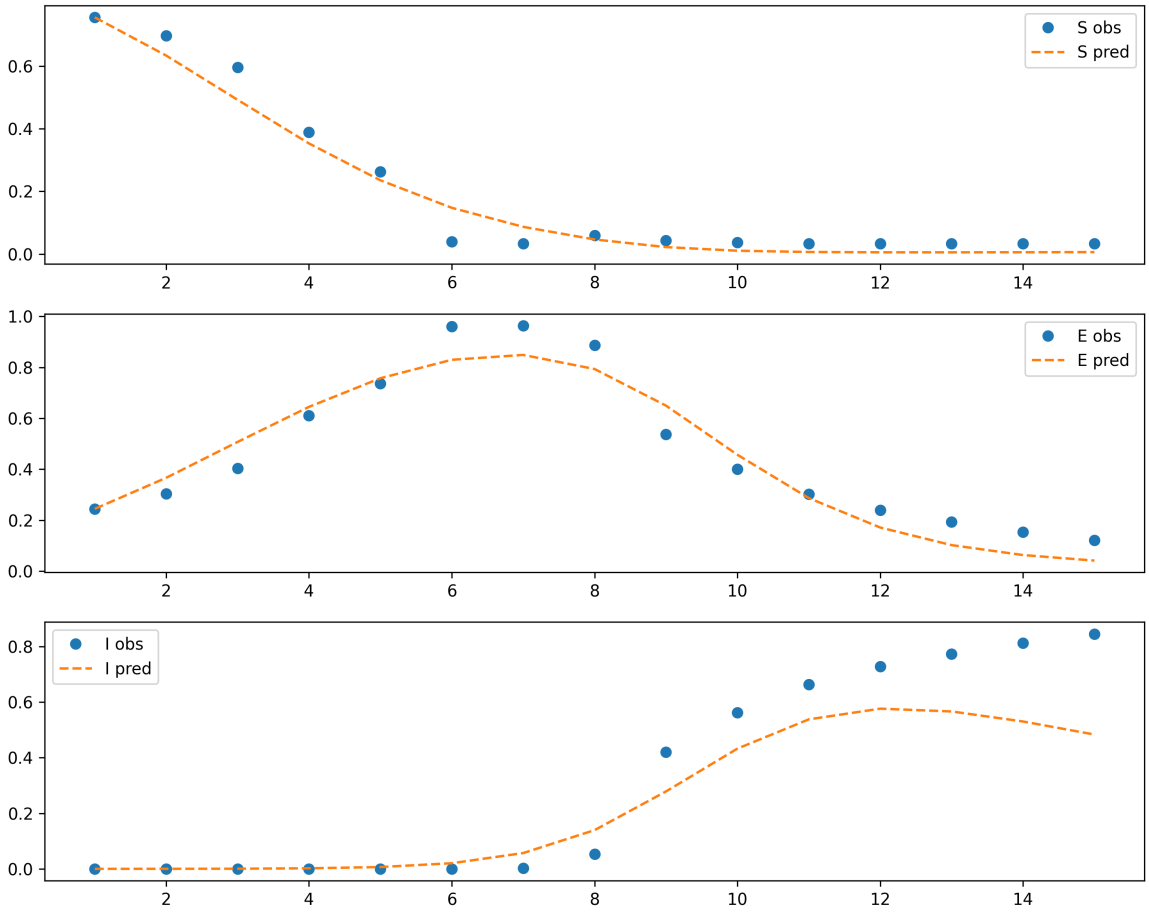

Figure 6. Fitted time-series curves.

The parameter $\sigma_{\max} = 0.6$ implies a minimal average latent period

$$\frac{1}{\sigma_{\max}} \approx 1.67 \text{ days}$$

during the most active stage of the disease. Since $\sigma(t)$ starts from small values and only approaches $\sigma_{\max}$ near τ, this corresponds to the biological interpretation that the latent disease remain physiologically quiescent for several days before a rapid transition into the infected.

Here, $\beta \approx 2.98$ is relatively high, reflecting the dense spore deposition in the controlled experimental setting. Moreover, $\theta \approx 0.20$ suggests that although the latent tissue contributes to secondary infection, its contribution is considerably smaller than that of infected tissue.

Finally, $\text{RMSE}_{\text{overall}} = 0.1028$ indicates that the model with $\sigma(t)$ can capture the essential qualitative characteristics and quantitative characteristics of the progression of SCR.

The high agreement between the observed data and the model's predictions validates the reliability of the model's parameters. Particularly, the model successfully reproduces the biological reality that $I(t)$ remains near zero during the first 6 days (latent phase) while $E(t)$ accumulates, followed by a rapid outbreak. This confirms that the calibrated model accurately reflects the actual physiological cycle of SCR from latent hyphal growth to sporulation.

5. Discussion

A model with a constant σ cannot match the two important features, namely the slow growth in the early stage and the subsequent rapid growth in the later stage, but the model with a time-varying $\sigma(t)$ can.

The results show that the latent stage of SCR is not time-homogeneous, but accelerates sharply at a specific threshold ($\tau \approx 9$ days). Furthermore, the small θ produced by fitting indicates that the contribution of latent tissue to the overall infection is limited, which means the infected tissue dominates the secondary spread. Together, these insights show that the non-autonomous extension of the SEI model provides a biologically realistic and quantitatively accurate representation of SCR.

Implications for disease management

- **Prioritize interventions before the logistic rise of** $\sigma(t)$. Because $\sigma(t)$ remains low from Day 1 to approximately Day 6 and rises sharply near Day 9, management measures are most effective during the early and slow-transition phase, which would significantly reduce the disease's severity.
- **Suppress early in the latent phase**. Although the symptomatic area dominates transmission, the model indicates that the latent pool grows to high levels before symptoms appear. Suppressing it early in the latent stage prevents the buildup of latent parts.
- **Reduce** β **via cultural and chemical measures**. The high value of β reflects a highly conducive environment, and measures such as increasing ventilation and reducing the duration of leaf wetness can lower β.
- **Delay the transition from the latent to the infectious stages**. Pesticide spraying can effectively reduce σ_{max} or shift τ to a later time.
- **Intensify monitoring during the transition period**. Since $\sigma(t)$ increases sharply around Day 8–10, measures should be taken during this period to determine the optimal spraying time.

Model comparison and limitations

To further evaluate the effectiveness of our proposed model, we compare it with the classical autonomous SEI model (where σ is constant) and traditional phenotypic analysis methods.

- **Comparison with the constant-parameter model:** As discussed in Section 5, the classical SEI model with a constant σ fails to capture the "latent-to-burst" transition characteristic of SCR. Our time-varying $\sigma(t)$ model significantly reduces the fitting error (RMSE = 0.1028) compared with the constant model, and effectively describes the sudden onset of symptoms after the latent period.
- **Comparison with traditional measurement:** Traditional methods rely on a visual estimation of disease severity, which is subjective and labor-intensive. In contrast, integrating the YOLOv11 semantic segmentation allows for objective, pixel-level quantification of the infected area $I(t)$, especially in distinguishing complex rust boundaries.

However, there are limitations to this study. The current model is validated using data from controlled artificial inoculation experiments. In complex field environments, the transmission rate β

and incubation period may be significantly affected by stochastic factors such as wind speed, rainfall, and temperature fluctuations, which are not yet explicitly included in the current equations. Future work will focus on incorporating these environmental variables into a non-autonomous system for field predictions.

Use of AI tools declaration

The authors declare they have not used Artificial Intelligence (AI) tools in the creation of this article.

Acknowledgments

The first author is supported by Joint Fund for Scientific and Technological Research and Development Plan in Henan Province (242103810029). Alain Miranville and Xinguang Yang were partially supported by the international communication project from the Department of Science and Technology in Henan province (No. 242102521039) and Workshop of Outstanding Foreign Scientists in Henan Province (No. GZS2024007).

Conflict of interest

Alain Miranville is editor-in-chief for Electronic Research Archive and was not involved in the editorial review or the decision to publish this article. All authors declare that there are no competing interests.

References

1. L. M. Underwood, Some new fungi chiefly from Alabama, *Bull. Torrey Bot. Club*, **24** (1897), 81–86. https://doi.org/10.2307/2477799
2. D. R. Duan, H. Z. He, Description of a rust *Puccinia polysora* on corn in Hainan Island, *Acta Mycol. Sin.*, **32** (1984), 125–126.
3. C. Casela, R. Renfro, A. F. Krattiger, Diagnosing maize diseases in Latin America, in *ISAAA Briefs No. 9*, ISAAA: Ithaca, NY and EMBRAPA, Brasilia, (1998), 57.
4. X. F. Liu, J. Y. Xu, Y. L. Gu, Q. Y. Sun, W. Y. Yuan, Z. H. Ma, Occurrence of *Puccinia polysora* causing southern corn rust in the northeast Huanghuaihai region of China, *Plant Dis.*, **102** (2018), 826. https://doi.org/10.1094/PDIS-05-17-0646-PDN
5. J. Liu, Y. Jiang, J. Zeng, G. Ji, L. Liu, K. Qiu, et al., Analysis of the severe occurrence characteristics and causes of southern corn rust in China in 2015, *China Plant Prot.*, **36**(2016), 44–47. https://doi.org/10.3969/j.issn.1672-6820.2016.05.011
6. J. Unartngam, P. Janruang, C. To-anan, Genetic diversity of *Puccinia polysora* in Thailand based on ISSR markers, *Int. J. Agric. Technol.*, **7** (2011), 1125–1137.
7. X. Yang, X. L. Ding, Z. L. He, Z. H. Ma, Determination of temperature required by southern corn rust, *Plant Prot.*, **41** (2015), 145–147. https://doi.org/10.3969/j.issn.0529-1542.2015.05.026

8. J. L. Brewbaker, S. K. Kim, Y. S. So, M. Logroño, H. G. Moon, R. Ming, et al., General resistance in maize to southern rust (*Puccinia polysora underw.*), *Crop Sci.*, **51** (2011), 1393–1409. https://doi.org/10.2135/cropsci2010.06.0327
9. S. Wang, R. Y. Zhang, Z. Shi, Y. X. Zhao, A. G. Su, Identification and fine mapping of RppM, a southern corn rust resistance gene in maize, *Front. Plant Sci.*, **11** (2020), 1057. https://doi.org/10.3389/fpls.2020.01057
10. L. M. Contreras-Medina, I. Torres-Pacheco, R. G. Guevara-González, R. J. Romero-Troncoso, I. R. Terol-Villalobos, R. A. Osornio-Rios, Mathematical modeling tendencies in plant pathology, *Afr. J. Biotechnol.*, **8** (2009), 7399–7408. https://doi.org/10.4314/ajb.v8i25
11. D. G. Jones, *The Epidemiology of Plant Diseases*, Kluwer Academic Publishers, Dordrecht, 1998.
12. L. V. Madden, Botanical epidemiology: some key advances and its continuing role in disease management, *Eur. J. Plant Pathol.*, **115** (2006), 3–23. https://doi.org/10.1007/s10658-005-1229-5
13. A. van Maanen, X. M. Xu, Modelling plant disease epidemics, *Eur. J. Plant Pathol.*, **109** (2003), 669–682. https://doi.org/10.1023/A:1026018005613
14. G. N. Agrios, *Plant Pathology*, Elsevier Academic Press, London, 2005.
15. T. Ji, I. Salotti, C. Dong, M. Li, V. Rossi, Modeling the effects of the environment and the host plant on the ripe rot of grapes, caused by the *Colletotrichum* species, *Plants*, **10** (2021), 2288. https://doi.org/10.3390/plants10112288
16. L. V. Madden, M. J. Jeger, F. van den Bosch, A theoretical assessment of the effects of vector-virus transmission mechanism on plant virus disease epidemics, *Phytopathology*, **90** (2000), 576–594. https://doi.org/10.1094/PHYTO.2000.90.6.576
17. M. Martcheva, *An Introduction to Mathematical Epidemiology*, Springer, New York, 2015. https://doi.org/10.1007/978-1-4899-7612-3
18. G. Wang, J. Yang, X. Li, An age-space structured cholera model linking within- and between-host dynamics with Neumann boundary condition, *Z. Angew. Math. Phys.*, **74** (2023), 14. https://doi.org/10.1007/s00033-023-02063-0
19. J. Yang, P. Jia, J. Wang, Z. Jin, Rich dynamics of a bidirectionally linked immuno-epidemiological model for cholera, *J. Math. Biol.*, **87** (2023), 71. https://doi.org/10.1007/s00285-023-02009-0
20. J. Wang, Mathematical models for cholera dynamics—A review, *Microorganisms*, **10** (2022), 2358. https://doi.org/10.3390/microorganisms10122358
21. C. Yang, J. Wang, On the intrinsic dynamics of bacteria in waterborne infections, *Math. Biosci.*, **296** (2018), 71–81. https://doi.org/10.1016/j.mbs.2017.12.005
22. H. Sha, L. Zhu, Dynamic analysis of pattern and optimal control research of rumor propagation model on different networks, *Inf. Process. Manage.*, **62** (2025), 104016. https://doi.org/10.1016/j.ipm.2024.104016
23. T. Yang, L. Zhu, S. Shen, L. He, Pattern dynamics analysis and parameter identification of spatiotemporal infectious disease models on complex networks, *Math. Biosci.*, **387** (2025), 109502. https://doi.org/10.1016/j.mbs.2025.109502

24. L. Zhu, T. Zheng, Pattern dynamics analysis and application of West Nile virus spatiotemporal models based on higher-order network topology, *Bull. Mathe. Biol.*, **87** (2025), 121. https://doi.org/10.1007/s11538-025-01501-6

25. P. van den Driessche, J. Watmough, Reproduction numbers and sub-threshold endemic equilibria for compartmental models of disease transmission, *Math. Biosci.*, **180** (2002), 29–48. https://doi.org/10.1016/S0025-5564(02)00108-6

26. W. Wang, X. Q. Zhao, Threshold dynamics for compartmental epidemic models in periodic environments, *J. Dyn. Differ. Equations*, **20** (2008), 699–717. https://doi.org/10.1007/s10884-008-9111-8

27. N. J. Cunniffe, R. O. J. H. Stutt, F. van den Bosch, C. A. Gilligan, ime-dependent infectivity and flexible latent and infectious periods in compartmental models of plant disease, *Anal. Theor. Plant Pathol.*, **102** (2012), 365–380. https://doi.org/10.1094/PHYTO-12-10-0338

28. C. A. Gilligan, An epidemiological framework for disease management, *Adv. Bot. Res.*, **38** (2002), 1–57. https://doi.org/10.1016/S0065-2296(02)38027-3

AIMS Press